LETTERS
PUBLISHED ONLINE: 25 AUGUST 2013 | DOI: 10.1038/NPHYS2702

nature physics

Ferromagnetic exchange, spin–orbit coupling and spiral magnetism at the $LaAlO_3/SrTiO_3$ interface

Sumilan Banerjee, Onur Erten and Mohit Randeria*

The electronic properties of the polar interface between insulating oxides is a subject of great interest[1–3]. An exciting development is the observation of robust magnetism[4–8] at the interface of two non-magnetic materials, $LaAlO_3$ (LAO) and $SrTiO_3$ (STO). Here we present a microscopic theory for the formation and interaction of local moments that depends on essential features of the LAO/STO interface. We show that correlation-induced moments arise owing to interfacial splitting of orbital degeneracy. We find that conduction electrons with a gate-tunable Rashba spin–orbit coupling mediate ferromagnetic exchange with a twist. We predict that the zero-field ground state is a long-wavelength spiral. Its evolution in an external field accounts semi-quantitatively for torque magnetometry data[5] and describes qualitative aspects of the scanning superconducting quantum interference device measurements[6]. We make several testable predictions for future experiments.

Recent experiments on the LAO/STO interface have seen tantalizing magnetic signals[4–8], often persisting up to high temperatures $\sim$100 K. A large magnetization of 0.3–0.4μ_B per interface Ti was observed by torque measurements[5] in an external field. In contrast, scanning superconducting quantum interference device (SQUID) experiments[6] found an inhomogeneous state with a dense set of local moments with no net magnetization, only isolated micron-scale ferromagnetic patches. Our goal is to reconcile these seemingly contradictory observations and to gain insight into the itinerant versus local moment nature of the magnetism, the exchange mechanism and the ordered state.

LAO and STO are both band insulators, but the TiO_2 layers at the interface are n-doped when LAO is terminated by a LaO^+ layer. The polar catastrophe[1] arising from a stack of charged LaO^+ and AlO_2^- layers grown on STO is averted by the transfer of 0.5 electrons per interface Ti. Oxygen vacancies are also known to provide additional electrons at the interface[1].

What is the fate of these electrons at the interface? Transport data suggest that only a small fraction of the electrons (5–10% of the 0.5 electrons per Ti) are mobile[2,9–11]. Interestingly, magneto-transport studies show a large, gate-tunable Rashba spin–orbit coupling (SOC) for these conduction electrons, arising from broken inversion at the interface[12]. Most of the electrons (comparable to 0.5 electrons per Ti) seem to behave like local moments in the magnetic measurements[5,6] discussed above.

We propose a microscopic model of electrons in Ti t_{2g} states at the LAO/STO interface that leads to the following results: local moments form in the top TiO_2 layer owing to correlations, with interfacial splitting of t_{2g} degeneracy playing a critical role; conduction electrons mediate ferromagnetic double-exchange interactions between the moments; Rashba SOC for the conduction electrons leads to a Dzyaloshinskii–Moriya interaction and a compass anisotropy term with a definite ratio of their strengths; the zero-field ground state is a long-wavelength spiral with a SOC-dependent pitch; the spiral transforms into a ferromagnetic state in an external field H.

We provide a semi-quantitative understanding of the torque results for the magnetization $M(H)$, and reconcile some of the key differences between the torque and SQUID measurements. We also point to a new magnetoelastic coupling effect that can be important for polar interfaces. Our model naturally explains the coexistence of magnetism and superconductivity at very low temperatures[5,6,8]. Finally, we make a number of specific predictions that can be tested experimentally.

Symmetry-based considerations

Many of our conclusions regarding magnetism can be understood qualitatively on the basis of symmetry alone. Although symmetry dictates the form of the interactions, the microscopic analysis shows how local moments $\mathbf{S_r}$ arise on a square lattice at the interface, and provides quantitative insights into the parameter dependence of exchange couplings. The isotropic Heisenberg exchange is $-J\sum_{\mathbf{r},\mu}\mathbf{S_r}\cdot\mathbf{S}_{\mathbf{r}+b\hat{\mu}}$, with $\hat{\mu}=\hat{x},\hat{y}$ and lattice spacing b. Its sign is not determined by symmetry, but our microscopic analysis leads to a ferromagnetic $J>0$. Inversion symmetry breaking at the interface implies two SOC terms: the Dzyaloshinskii–Moriya interaction $D\sum_{\mathbf{r},\mu}\hat{d}_\mu\cdot(\mathbf{S_r}\times\mathbf{S}_{\mathbf{r}+b\hat{\mu}})$ with $\hat{d}_\mu=\hat{z}\times\hat{\mu}$, and the compass anisotropy $-\sum_{\mathbf{r}}[A'(S^x_{\mathbf{r}}S^x_{\mathbf{r}+b\hat{x}}+S^y_{\mathbf{r}}S^y_{\mathbf{r}+b\hat{y}})+A(S^x_{\mathbf{r}}S^x_{\mathbf{r}+b\hat{y}}+S^y_{\mathbf{r}}S^y_{\mathbf{r}+b\hat{x}})]$.

One can see, quite generally, that the ground state of such a model can be a long-wavelength spiral that looks locally ferromagnetic, thus minimizing the J term, with pitch determined by the Dzyaloshinskii–Moriya term. Our microscopic results for D, A, A' unequivocally predict such a spiral state for $H=0$, which turns into an in-plane ferromagnet for $H\gtrsim 1$ T. These observations permit us to understand the torque data in a field[5] semi-quantitatively, and to see why over most of the sample the $H=0$ scanning SQUID measurements find no net moment[6].

Electronic structure

Both density functional theory[13,14] (DFT) and spectroscopy[15–17], show that, in the top TiO_2 layer d_{xy} states have lower energy than d_{xz}, d_{yz} (Fig. 1a). In addition to z confinement raising the xz, yz levels, the mismatch of in-plane LAO and STO lattice parameters leads to an out-of-plane distortion that lowers d_{xy}. The d_{xy} orbitals delocalize primarily in the x–y plane, and similarly for d_{xz} and d_{yz}. DFT (refs 18,19) and photoemission[20] find the in-plane hopping between d_{xy} orbitals $t\simeq 0.3$ eV, whereas the out-of-plane $t'\simeq t/30$. The resulting xz (yz) bands are quasi-one-dimensional (1D), dispersing primarily along x (y), and confined along z.

Department of Physics, The Ohio State University, Columbus, Ohio 43210, USA. *e-mail: randeria@mps.ohio-state.edu

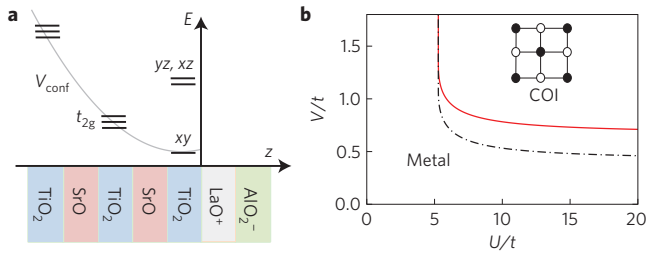

Figure 1 | Electronic orbitals and charge localization. a, Schematic of Ti t_{2g} energy levels. At the interface d_{xy} is lower than the d_{yz} and d_{xz} orbitals. $V_{conf}(z)$ is the confining potential. **b**, Phase diagram of the single-band extended Hubbard model at quarter-filling. A COI is obtained for moderate values of on-site Hubbard U and next-neighbour Coulomb V, above the (solid red) phase boundary. Coupling to the breathing-mode phonon further stabilizes the COI. The dashed black line corresponds to an energy gain $E_{ph} = 0.25t$ due to lattice distortion (see Methods).

Local moments

Coulomb interactions, disorder and coupling to phonons can all play a role in localizing charge. Nevertheless, interactions are essential for forming local moments. Experiments[11,21] show that the quasi-1D xz, yz bands, which should be the most sensitive to disorder, contribute to transport, ruling out Anderson localization. We thus make a simple model where we treat correlations first and can then add the effects of phonons and disorder.

The key to understanding correlation effects is the splitting of t_{2g} degeneracy at the interface that leads to a quarter-filled xy band (0.5 electrons per Ti) in the top TiO_2 layer. A modest on-site Hubbard U and next-neighbour Coulomb V then lead to a charge-ordered insulator (COI; Fig. 1b). We obtain a simple analytical result for the metal–insulator transition using a slave-rotor approach[22]. Coupling to the breathing-mode phonon further stabilizes the COI; (see Methods). DFT calculations need a rather large $U \simeq 8$ eV to stabilize a COI (ref. 23). We see from Fig. 1 that, for realistic values[24] of $U = 4$ eV ($U/t \simeq 13$) and $V \simeq 0.5$–1 eV ($V/t \simeq 1.5$–3), we are deep in the chequerboard COI state.

Exchange

Consider then the problem of local moments in d_{xy} orbitals on a chequerboard lattice (Fig. 2a) interacting through Hund's coupling J_H with a small density n_c of conduction electrons in xz, yz bands. Given $J_H \simeq 1$ eV, it is much more reasonable to work in the non-perturbative double-exchange limit $J_H \gg t$ than in the perturbative RKKY limit $J_H \ll t$. We treat the $S = 1/2$ moments classically. This is justified *a posteriori* because of the small quantum fluctuations in the ferromagnetic and long-wavelength spiral states.

We find $\mathcal{H}_{eff} = \sum_{\mathbf{r}}[\mathcal{H}_x(\mathbf{r}) + \mathcal{H}_y(\mathbf{r})] + \mathcal{H}'$ with

$$\mathcal{H}_x(\mathbf{r}) = -J\mathbf{S}_{\mathbf{r}} \cdot \mathbf{S}_{\mathbf{r}+2\hat{x}} - AS^y_{\mathbf{r}} S^y_{\mathbf{r}+2\hat{x}} - D\hat{y} \cdot (\mathbf{S}_{\mathbf{r}} \times \mathbf{S}_{\mathbf{r}+2\hat{x}}) \qquad (1)$$

where $\mathbf{r}$ denotes positions of occupied sites in the COI (see Methods). $\mathcal{H}_y(\mathbf{r})$ is obtained by interchanging $x \leftrightarrow y$ and replacing $D \to -D$ in $\mathcal{H}_x(\mathbf{r})$. The term $\mathcal{H}' = -J' \sum_{\mathbf{r}} \mathbf{S}_{\mathbf{r}} \cdot (\mathbf{S}_{\mathbf{r}+\hat{x}+\hat{y}} + \mathbf{S}_{\mathbf{r}+\hat{x}-\hat{y}})$ couples nearest neighbours along the diagonal (Fig. 2a). The spins have normalization $\mathbf{S}^2_{\mathbf{r}} = 1$. The form of $\mathcal{H}_x$ and $\mathcal{H}_y$, as well as $J \gg J'$, arises from the two-sublattice structure of the COI and the quasi-1D nature of xz, yz bands. We find $J \simeq n_c t/4$ and $J' \simeq n_c t'/4$ for low carrier density n_c (the number of electrons per Ti in each band).

The new aspect here is the Rashba SOC $2\lambda a\hat{z} \cdot (\mathbf{k} \times \boldsymbol{\sigma})$ for the conduction electrons, where $\mathbf{k}$ is their momentum, $\boldsymbol{\sigma}$ are Pauli matrices and a is the Ti–Ti distance. The SOC strength λ is determined by the electric field at the interface. Experiments[12] find a gate-voltage-tunable $\lambda \simeq 1.3$–6.3 meV ($\lambda/t \simeq 0.004$–0.022). SOC then gives rise to the Dzyaloshinskii–Moriya and compass terms in $\mathcal{H}_{eff}$ through the double-exchange mechanism. For $\lambda/t \ll 1$, we find $D \simeq n_c\lambda$, $A \simeq 2n_c\lambda^2/t$ and $A' = 0$. Thus, $D/J \sim \lambda/t$ and $A/J \sim (\lambda/t)^2$ with $AJ/D^2 = 1/2$ independent of parameters.

Spiral ground state

We have examined the ground-state properties of $\mathcal{H}_{eff}$ in an external field $\mathbf{H}$ using a variety of techniques. Using a variational approach we find that, for $AJ/D^2 < 1$, the $H = 0$ ground state is

$$\mathbf{S}_{\mathbf{r}} = \sin(\mathbf{Q}_0 \cdot \mathbf{r})\hat{\mathbf{Q}}_0 + \cos(\mathbf{Q}_0 \cdot \mathbf{r})\hat{z} \qquad (2)$$

a coplanar spiral with spins lying in a plane perpendicular to the interface. Here $\mathbf{Q}_0 = (2\lambda/ta)(\cos\varphi\,\hat{x} + \sin\varphi\,\hat{y})$; see Methods. For $AJ/D^2 > 1$, the ground state is an in-plane ferromagnet with $\mathbf{S}_{\mathbf{r}} = \cos\varphi\,\hat{x} + \sin\varphi\,\hat{y}$. For all AJ/D^2, the ground state is infinitely degenerate (arbitrary $0 \le \varphi < 2\pi$), even though $\mathcal{H}_{eff}$ has $\mathbb{Z}_4$ symmetry. This peculiar degeneracy of compass anisotropy[25] is expected to be broken by order-by-disorder.

The microscopic value $AJ/D^2 = 1/2$ implies a zero-field spiral variational ground state. We have verified the stability of the spiral at $H = 0$ using two independent, unbiased calculations (see Supplementary Information): finite-temperature Monte Carlo and $T = 0$ conjugate gradient energy minimization. In Fig. 2b we show an example of spiral ordering in real space with a wavelength of a few lattice spacings. For realistic values of $\lambda/t \sim 0.02$, our variational results give a pitch of $(2\pi/Q_0) \sim 600$ Å.

In Fig. 2c–h, we show the evolution of the spiral state as a function of $\mathbf{H}$ applied in the x–z plane at an angle $\theta_H = 15°$ with the z axis, (the geometry used in the torque experiments[5]). In the variational calculation (Fig. 2c) the spiral state ($\mathbf{Q} \neq 0$) develops into a fully magnetized state above a field H_{peak}, which corresponds to a maximum in the in-plane component M_x of $\mathbf{M} = \langle \mathbf{S}_{\mathbf{r}} \rangle$. We plot in Fig. 2d,e M_x and M_z as functions of H, where we also see excellent agreement between variational and Monte Carlo results. For the Monte Carlo simulations we used larger SOC $\lambda/t = \pi/25$ that led to smaller pitch spirals. Below we use realistic SOC λ values to study long-wavelength spirals within a variational approach.

The evolution from spiral to ferromagnet as a function of field is best seen in the spin structure factor $I_{\mathbf{q}} \propto |\langle \mathbf{S}_{\mathbf{q}} \rangle|^2$ shown in Fig. 2f–h, where $\mathbf{S}_{\mathbf{q}}$ is the Fourier transform of $\mathbf{S}_{\mathbf{r}}$. The spiral at $H = 0$ shows two peaks in $I_{\mathbf{q}}$ at $\mathbf{q} = \pm Q_0\hat{y}$ (Fig. 2f), which lie on the white circle, the locus of $\mathbf{Q}_0$ corresponding to the degenerate states in equation (2). At intermediate fields, a uniform component develops along with $\mathbf{q} \neq 0$ peaks (Fig. 2g), whereas for $H > H_{peak}$ one obtains a ferromagnet (Fig. 2h).

Torque and magnetization

The torque $\boldsymbol{\tau} = \mathbf{M} \times \mathbf{H}$ is non-zero only in the presence of spin-space anisotropy, otherwise $\mathbf{M}$ would simply align with $\mathbf{H}$. In Fig. 3a, we compare our variational results with the magnetization $M_\tau \equiv \tau/H$ versus H derived from torque magnetometry[5], where M_τ is the component of $\mathbf{M}$ perpendicular to $\mathbf{H}$. (The experimental data have been shown after background subtraction; see Supplementary Information.)

The $\mathbf{M}(\mathbf{H})$ curve shows no hysteresis[5], because the spiral state has no spontaneous magnetization at $H = 0$. The in-plane component of the field ($\theta_H \neq 0$) induces a uniform magnetization in the spiral state (Fig. 2). This leads to an increasing M_τ for $H < H_{peak}$ in Fig. 3a, where H_{peak}, at which M_τ is a maximum, depends on θ_H. For $H > H_{peak}$, the ground state is a ferromagnet (Fig. 2) with the compass term giving rise to a large easy-plane anisotropy $A \simeq 0.15$–0.3 T (with $\lambda \simeq 0.016$–0.022 and $n_c = 0.05$) that tries to keep $\mathbf{M}$ in the plane. For large enough H the field dominates over the anisotropy, pulls $\mathbf{M}$ out of the plane and M_τ decreases. These two regimes are shown schematically in Fig. 3a inset.

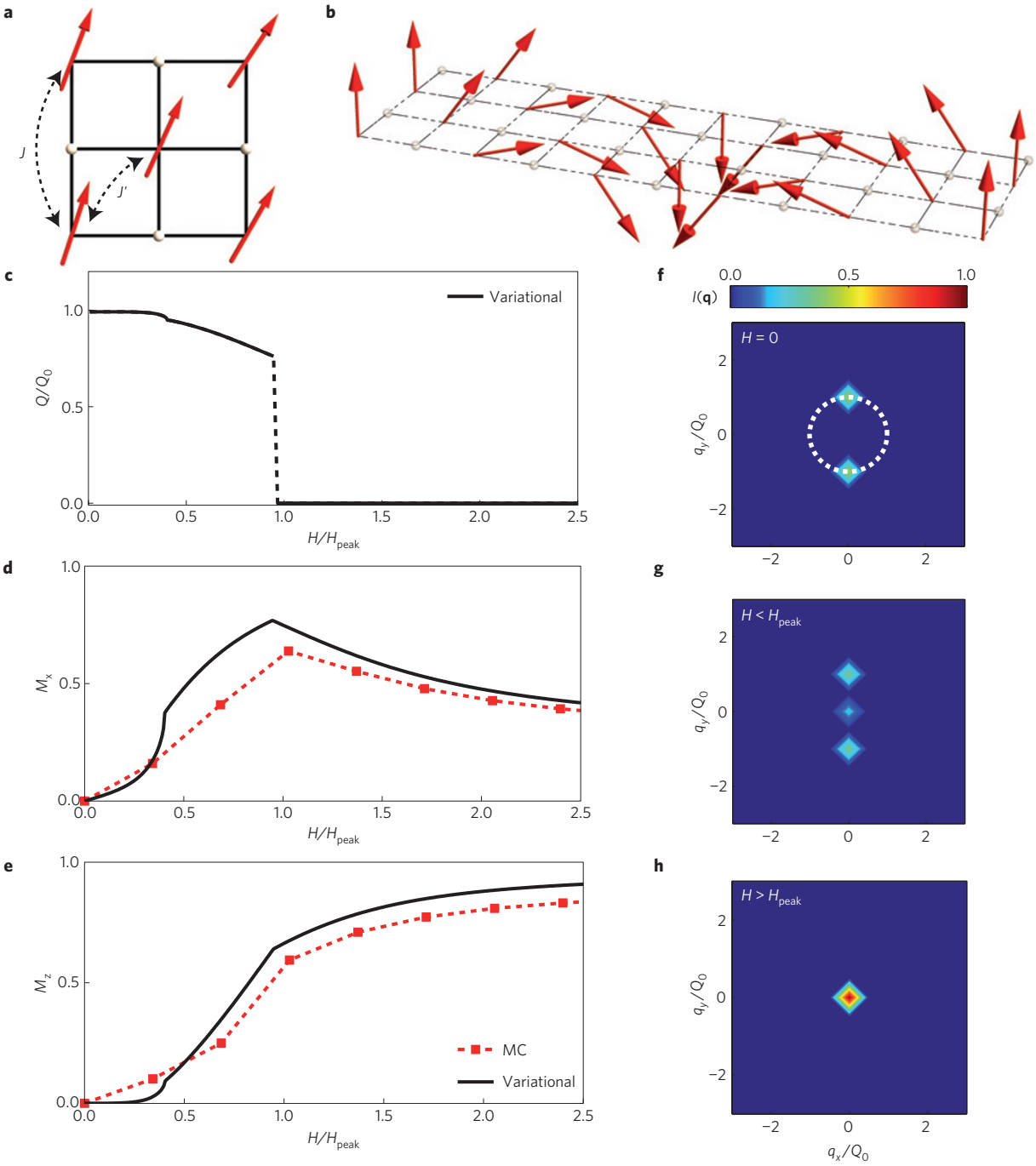

Figure 2 | Spiral ground state and its evolution with field. a, Local moments in the COI with ferromagnetic exchange J and J'. Anisotropy and Dzyaloshinskii–Moriya terms couple the same spins as J. **b**, The zero-field spiral ground state, whose evolution with $\mathbf{H} = H(\sin\theta_H\hat{x} + \cos\theta_H\hat{z})$ with $\theta_H = 15°$ is shown next. **c**, The H dependence of the spiral Q normalized by its $H = 0$ value Q_0 for SOC $\lambda/t = \pi/25$. **d**,**e** In-plane (M_x; **d**) and out-of-plane (M_z; **e**) components of the magnetization obtained from $T = 0$ variational calculations and $T = 0.25J$ Monte Carlo (MC) simulations. The H axis is scaled by H_{peak} at which M_x has a maximum. Panels **f**–**h** show the Monte Carlo spin structure factor $I(\mathbf{q})$. **f**, At $H = 0$ the peaks of $I(\mathbf{q})$ lie on a white circle, the locus of $\mathbf{Q}_0$ corresponding to degenerate variational ground states. **g**, For $0 < H < H_{peak}$, the $I(\mathbf{q})$ shows a net ferromagnetic moment in addition to spiral peaks. **h**, A ferromagnetic state is obtained for $H > H_{peak}$.

In Fig. 3a we show two $M(H)$ curves that differ in their choice of AJ/D^2. The red curve with $AJ/D^2 = 1/2$ has too rapid a high-field drop in $M_\tau(H)$. (Here $A = 2n_c\lambda^2/t = 0.3$ is tuned to match H_{peak} and $\lambda/t = 0.022$, $n_c = 0.05$.) The blue curve with $AJ/D^2 = 0.8$ (with $\lambda/t = 0.028$) leads to better agreement with experiment. Such a phenomenological choice of AJ/D^2 amounts to changing the anisotropy while keeping Dzyaloshinskii–Moriya fixed. Although A and D were both determined by Rashba SOC in our microscopic theory, dipolar interactions and atomic SOC also contribute to A (see Supplementary Information).

The peak position $H_{peak} \propto n_c\lambda^2/t$ in our microscopic model and $M_\tau(H)$ for different λ collapse onto a single curve when plotted versus H/H_{peak} (see Fig. 3b,c). In practice, other sources of anisotropy might modify this scaling. Nevertheless, both n_c and λ are gate tunable and we expect H_{peak} to vary substantially with bias.

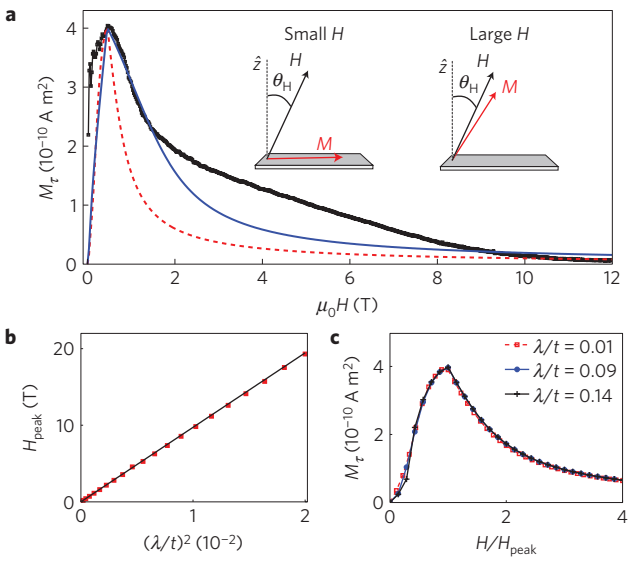

Figure 3 | Torque magnetometry. a, Magetization $M_\tau = \tau/H$ (black symbols) from torque experiments[5] at $T = 300$ mK with $\theta_H = 15°$; (see Supplementary Information for background subtraction). Theoretical $M_\tau(H)$ (red curve) computed with microscopic value $AJ/D^2 = 1/2$ with $A \simeq 0.3$ T chosen to match H_{peak}. Better agreement (blue curve) with experiment is obtained by the phenomenological choice $AJ/D^2 = 0.8$ with $A \simeq 0.7T$. The inset shows a schematic of two regimes in torque: an in-plane net magnetization **M** for small H evolving into a out-of-plane **M** for large H. **b**, H_{peak} scales with $(\lambda/t)^2$ for fixed n_c, as predicted by the microscopic model. **c**, $M_\tau(H)$ curves, with different SOC that can be tuned by gating, collapse onto a single curve versus H/H_{peak}.

Scanning SQUID experiments

We now discuss how we can reconcile the torque[5] and scanning SQUID (ref. 6) results. At $H = 0$ most of the sample has spiral order and hence no net magnetization, consistent with ref. 6. A detailed modelling of the observed inhomogeneity is beyond the scope of this paper, nevertheless we can offer a plausible picture based on our theory. The energy gain of spiral over ferromagnet is quite small: $\Delta\epsilon \simeq (D^2/J - A)/2 = n_c\lambda^2/t \simeq$ 0.1–0.2 K. Therefore, small terms ignored up to now might well upset the balance in favour of the ferromagnet. We find that magnetoelastic coupling to polar distortions, a new aspect of these interfaces, can reverse the balance between spiral and ferromagnetic states and stabilize ferromagnetic patches (see Methods). These ferromagnetic patches can then point in any in-plane direction, consistent with compass anisotropy.

Discussion

We comment briefly on how our theory, which builds on insights from DFT (refs 13,18,19,23), differs from other approaches. It is hard to obtain the large exchange or net moment seen in LAO/STO from itinerant models[26], which may be relevant for $GdTiO_3/SrTiO_3$. On symmetry grounds, these itinerant systems will also have a SOC-induced spiral ground state similar to the one discussed here. Our model differs from ref. 27 in several respects. We are in the non-perturbative double-exchange limit and not the RKKY regime. In our model, xz, yz carriers mediate exchange. The xy electrons in lower layers have essentially no interaction with moments in the xy orbitals of the top TiO_2 layer. This results from the small overlap t' between xy orbitals along $\hat{z}$ as well as the level mismatch due to confinement. Conventional superconductivity arises in xy states in lower layers and is decoupled from the local moments.

Conclusions

Our theory has several testable predictions. Local moment formation is associated with (π,π) charge order at the interface, although disorder will probably disrupt the order. The zero-field state is predicted to be a coplanar spiral state with several striking properties, including a wave vector that scales linearly with Rashba SOC and hence is gate tunable. The evolution from a spiral to a ferromagnetic state in an external field has characteristic signatures in the spin structure factor. The easy-plane anisotropy strength is also dominated by SOC and exhibits substantial gate voltage dependence that can be tested in torque magnetometry experiments. The ferromagnetic exchange $J = n_c t/4 \simeq 40$ K (for $n_c = 0.05$ and $t = 0.3$ eV) should also be tunable by changing n_c, the density of carriers. A theoretical analysis of the finite temperature properties of our model is left for future investigations.

Methods

Charge-ordering Mott transition. We consider the quarter-filled, extended Hubbard model on a 2D square lattice with onsite U and nearest-neighbour Coulomb V. Using slave-rotor[22] mean field theory for U and Hartree–Fock for V, we obtain an analytical result for the transition from metal to charge ordered insulator (COI). The chequerboard COI is stable for $U > 8\langle t\rangle$ when $U < 4V$, and for $(U-2V)V/U > \langle t\rangle$ when $U > 4V$. Here $\langle t\rangle \simeq 0.66t$ is the kinetic energy of occupied states. Slave-rotor mean field theory has been found to be in excellent semi-quantitative agreement with dynamical mean field theory for several problems. In fact, our 2D square lattice results are quite similar to dynamical mean field theory of the Wigner–Mott transition on a Bethe lattice[28].

The COI is stabilized by coupling to the breathing-mode phonon, which has the same (π,π) wave vector as the charge order (see Supplementary Information). The only change above is that $V \to \widetilde{V} = V + E_{ph}$, where E_{ph} is the energy gained though lattice distortion. Typical values of $E_{ph} \simeq 0.05$–0.10 eV (ref. 29).

Double exchange. The local moments $\mathbf{S}_\mathbf{r}$ on the sites of a 2D chequerboard lattice are described by their orientation $(\theta_\mathbf{r}, \varphi_\mathbf{r})$. In the large J_H limit, a conduction electron on the local-moment sublattice (a) has its spin parallel to $\mathbf{S}_\mathbf{r}$. Thus, we write the spin-full fermion operators $\tilde{a}_{\mathbf{r}\alpha\sigma}$, with orbital index $\alpha = (xz), (yz)$, in terms of spinless fermions $a_{\mathbf{r}\alpha}$, through $\tilde{a}^\dagger_{\mathbf{r}\alpha\sigma} \to F_{r\sigma}a^\dagger_{r\alpha}$. Here $F_{\mathbf{r}\uparrow} = \cos(\theta_\mathbf{r}/2)$ and $F_{\mathbf{r}\downarrow} = \sin(\theta_\mathbf{r}/2)e^{-i\varphi_\mathbf{r}}$.

Both spin projections $\sigma = \uparrow, \downarrow$ are allowed on empty sublattice (b) sites, for which we use a common (global) quantization axis. The kinetic energy is then given by

$$\mathcal{H}_K = -\sum_{\mathbf{r},\alpha,\hat{\mu},\sigma} t_{\alpha\hat{\mu}} F_{\mathbf{r}\sigma} a^\dagger_{\mathbf{r}\alpha}(b_{\mathbf{r}+\hat{\mu},\alpha\sigma} + b_{\mathbf{r}-\hat{\mu},\alpha\sigma}) + \text{h.c.}$$

where $t_{(xz),\hat{x}} = t_{(yz),\hat{y}} = t$ and $t_{(xz),\hat{y}} = t_{(yz),\hat{x}} = t' \simeq t/30$.

The Rashba terms $\sigma^x \sin(k_y a) \sim -k_y a(\boldsymbol{\sigma}\times\hat{z})_y$ and $\sigma^y \sin(k_x a) \sim k_x a(\boldsymbol{\sigma}\times\hat{z})_x$ lead to the SOC Hamiltonian

$$\begin{aligned}\mathcal{H}_R = i\lambda \sum_{\mathbf{r},ij} [&\sigma^x_{ij}\tilde{a}^\dagger_{\mathbf{r}(yz)i}(b_{\mathbf{r}+\hat{y},(yz)j} - b_{\mathbf{r}-\hat{y},(yz)j}) \\ &-\sigma^y_{ij}\tilde{a}^\dagger_{\mathbf{r}(xz)i}(b_{\mathbf{r}+\hat{x},(xz)j} - b_{\mathbf{r}-\hat{x},(xz)j})] + \text{h.c.}\end{aligned}$$

We can rewrite this in terms of the spinless a fermions as

$$\mathcal{H}_R = \sum_{\mathbf{r}\alpha\sigma} [\lambda_{\alpha\sigma} F_{\mathbf{r}\bar{\sigma}} a^\dagger_{\mathbf{r}\alpha}(b_{\mathbf{r}+\hat{\mu},\alpha\sigma} - b_{\mathbf{r}-\hat{\mu},\alpha\sigma})] + \text{h.c.}$$

where $\bar{\sigma} = -\sigma$ and we define $\lambda_{(xz)\uparrow} = -\lambda_{(xz)\downarrow} = \lambda$ and $\lambda_{(yz)\uparrow} = \lambda_{(yz)\downarrow} = i\lambda$.

To obtain the parameters J, J', D and A of $\mathcal{H}_{eff}$ of equation (1) starting from the microscopic $\mathcal{H}_{DE} = \mathcal{H}_K + \mathcal{H}_R$, we match the energies of several low-lying configurations computed for both $\mathcal{H}_{DE}$ and $\mathcal{H}_{eff}$. See Supplementary Information for details.

Variational calculation. We study the ground-state properties of $\mathcal{H}_{eff}$ using a variational ansatz $\mathbf{S}_\mathbf{r} = \mathbf{M} + \mathbf{R}(\mathbf{Q})\cos(\mathbf{Q}\cdot\mathbf{r}) + \mathbf{I}(\mathbf{Q})\sin(\mathbf{Q}\cdot\mathbf{r})$ with $\mathbf{Q} \neq 0$. The normalization $\mathbf{S}_r^2 = 1$ is satisfied by the constraints $\mathbf{M}\cdot\mathbf{R} = \mathbf{M}\cdot\mathbf{I} = \mathbf{R}\cdot\mathbf{I} = 0$; $\mathbf{R}^2 = \mathbf{I}^2$ and $\mathbf{M}^2 + \mathbf{R}^2 = 1$. We numerically minimize the energy per spin ϵ to obtain optimal values for $\mathbf{M}$, $\mathbf{R}$, $\mathbf{I}$ and $\mathbf{Q}$ as a function of $\mathbf{H}$, and calculate the torque.

At zero field, we find a spiral ground state of equation (2) with $\mathbf{Q} = \mathbf{Q}_0$ and $\mathbf{M} = 0$ for $AJ/D^2 < 1$ and an in-plane ferromagnet for $AJ/D^2 > 1$. We can see this analytically using the ansatz $\mathbf{S}_\mathbf{r} = \mathbf{R}\cos(\mathbf{Q}\cdot\mathbf{r}) + \mathbf{I}\sin(\mathbf{Q}\cdot\mathbf{r})$. We write $\mathbf{R} = \sin\theta\sin\varphi\hat{x} - \sin\theta\cos\varphi\hat{y} + \cos\theta\hat{z}$ and $\mathbf{I} = \cos\varphi\hat{x} + \sin\varphi\hat{y}$ with $\theta \in [0,\pi]$ and $\varphi \in [0, 2\pi)$. We first minimize with respect to $\mathbf{Q}$ (for $Qa \ll 1$), find the optimal $\mathbf{Q} = (D/2Ja)\cos\theta(\cos\varphi\hat{x} + \sin\varphi\hat{y})$ and the energy

$\epsilon(\mathbf{Q}) \simeq -2(J+J') - A + (A - D^2/J)(\cos^2\theta)/2$, which is independent of φ. For $AJ/D^2 < 1$, the optimal choice of $\cos\theta = 1$ leads to the spiral of equation (2) with $\mathbf{Q} = \mathbf{Q}_0$ and an energy gain $\Delta\epsilon = (D^2/J - A)/2$ relative to the ferromagnetic state. For our microscopic model $\Delta\epsilon = n_c\lambda^2/t$.

Polar distortions. Displacements $u\hat{z}$ of oxygen ions that bridge Ti–O–Ti bonds[30] at the interface affect the local electric field and hence the Rashba SOC $\lambda(u) = \lambda - \lambda_1 u$. Here $\lambda_1 > 0$ because the local electric field decreases if negatively charged oxygen ions move up ($u > 0$). The resulting coupling to magnetism can be modelled by $A \to A(u) = 2n_c\lambda^2(u)/t$ and $D \to D(u) = n_c\lambda(u)$ in the energy $\epsilon(\mathbf{Q})$, in addition to the cost of distortion. The A and D terms in $\mathcal{H}_{\text{eff}}$ gain energy by increasing $\lambda(u)$ with $u < 0$. However, this costs an electrostatic energy $-qEu$ and an elastic energy $Ku^2/2$, where $\mathbf{E} = -E\hat{z}$ is the electric field acting on oxygen ions at the interface and K is the elastic constant. We minimize the total energy with respect to u to find that energy gain of the spiral is reduced: $\Delta\epsilon \simeq (n_c\lambda^2/t)[1 - 2qE\lambda_1/K\lambda]$. With suitable choice of parameters, one can make $\Delta\epsilon < 0$ and stabilize the ferromagnetic state over the spiral.

Received 25 March 2013; accepted 17 June 2013; published online 25 August 2013

References

1. Ohtomo, A. & Hwang, H. Y. A high-mobility electron gas at the $LaAlO_3/SrTiO_3$ heterointerface. *Nature* **427,** 423–426 (2004).
2. Thiel, S., Hammerl, G., Schmehl, A., Schneider, C. W. & Mannhart, J. Tunable quasi two-dimensional electron gases in oxide heterostructures. *Science* **313,** 1942–1945 (2006).
3. Zubko, P., Gariglio, S., Gabay, M., Ghosez, P. & Triscone, J-M. Interface physics in complex oxide heterostructures. *Annu. Rev. Condens. Matter Phys.* **2,** 141–165 (2011).
4. Brinkman, A. *et al.* Magnetic effects at the interface between non-magnetic oxides. *Nature Mater.* **6,** 493–496 (2007).
5. Li, L., Richter, C., Mannhart, J. & Ashoori, R. C. Coexistence of magnetic order and two-dimensional superconductivity at $LaAlO_3/SrTiO_3$ interfaces. *Nature Phys.* **7,** 762–766 (2011).
6. Bert, J. *et al.* Direct imaging of the coexistence of ferromagnetism and superconductivity at the $LaAlO_3/SrTiO_3$ interface. *Nature Phys.* **7,** 767–771 (2011).
7. Ariando, *et al.* Electronic phase separation at the $LaAlO_3/SrTiO_3$ interface. *Nature Commun.* **2,** 188–194 (2011).
8. Dikin, D. A., Mehta, M., Bark, C. W., Folkman, C.M., Eom, C. B. & Chandrasekhar, V. Coexistence of superconductivity and ferromagnetism in two dimensions. *Phys. Rev. Lett.* **107,** 56802–56805 (2011).
9. Shalom, M. B., Ron, A., Palevski, A. & Dagan, Y. Shubnikov-De Haas oscillations in $SrTiO_3/LaAlO_3$ interface. *Phys. Rev. Lett.* **105,** 206401 (2010).
10. Lerer, S., Shalom, M. B., Deutscher, G. & Dagan, Y. Low-temperature dependence of the thermomagnetic transport properties of the $SrTiO_3/LaAlO_3$ interface. *Phys. Rev. B* **84,** 075423 (2011).
11. Joshua, A., Pecker, S., Ruhman, J., Altman, E. & Ilani, S. A universal critical density underlying the physics of electrons at the $LaAlO_3/SrTiO_3$ interface. *Nature Commun.* **3,** 1129 (2012).
12. Caviglia, A. D., Gabay, M., Gariglio, S., Reyren, N., Cancellieri, C. & Triscone, J-M. Tunable Rashba spin-orbit interaction at oxide interfaces. *Phys. Rev. Lett.* **104,** 126803 (2010).
13. Pentcheva, R. & Pickett, W. E. Charge localization or itineracy at $LaAlO_3/SrTiO_3$ interfaces: Hole polarons, oxygen vacancies, and mobile electrons. *Phys. Rev. B* **74,** 035112 (2006).
14. Delugas, P. *et al.* Spontaneous 2-dimensional carrier confinement at the *n*-type $SrTiO_3/LaAlO_3$ interface. *Phys. Rev. Lett.* **106,** 166807 (2011).
15. Salluzzo, M. *et al.* Orbital reconstruction and the two-dimensional electron gas at the $LaAlO_3/SrTiO_3$ interface. *Phys. Rev. Lett.* **102,** 166804 (2009).
16. Sing, M. *et al.* Profiling the interface electron gas of $LaAlO_3/SrTiO_3$ heterostructures with hard x-ray photoelectron spectroscopy. *Phys. Rev. Lett.* **102,** 176805 (2009).
17. Berner, G. *et al.* $LaAlO_3/SrTiO_3$ oxide heterostructures studied by resonant inelastic x-ray scattering. *Phys. Rev. B* **82,** 241405 (2010).
18. Popovic, Z. S., Satpathy, S. & Martin, R. M. Origin of the two-dimensional electron gas carrier density at the $LaAlO_3$ on $SrTiO_3$ interface. *Phys. Rev. Lett.* **101,** 256801 (2008).
19. Hirayama, M., Miyake, T. & Imada, M. *Ab initio* Low-energy model of transition-metal-oxide heterostructure $LaAlO_3/SrTiO_3$. *J. Phys. Soc. Jpn* **81,** 084708 (2012).
20. Santander-Syro, A. F. *et al.* Two-dimensional electron gas with universal subbands at the surface of $SrTiO_3$. *Nature* **469,** 189–194 (2011).
21. Fête, A., Gariglio, S., Caviglia, A. D., Triscone, J-M. & Gabay, M. Rashba induced magnetoconductance oscillations in the $LaAlO_3$–$SrTiO_3$ heterostructure. *Phys. Rev. B* **86,** 201105 (2012).
22. Florens, S. & Georges, A. Slave-rotor mean-field theories of strongly correlated systems and the Mott transition in finite dimensions. *Phys. Rev. B* **70,** 035114 (2004).
23. Pentcheva, R. & Pickett, W. E. Ionic relaxation contribution to the electronic reconstruction at the *n*-type $LaAlO_3/SrTiO_3$ interface. *Phys. Rev. B* **78,** 205106 (2008).
24. Imada, M., Fujimori, A. & Tokura, Y. Metal-insulator transitions. *Rev. Mod. Phys.* **70,** 1039–1263 (1998).
25. Nussinov, Z., Biskup, M., Chayes, L. & van den Brink, J. Orbital order in classical models of transition-metal compounds. *Eur. Phys. Lett.* **67,** 990–996 (2004).
26. Chen, G & Balents, L. Ferromagnetism in itinerant two-dimensional t_{2g} systems. *Phys. Rev. Lett.* **110,** 206401 (2013).
27. Michaeli, K, Potter, A. C. & Lee, P. A. Superconducting and ferromagnetic phases in $SrTiO_3/LaAlO_3$ oxide interface structures: possibility of finite momentum pairing. *Phys. Rev. Lett.* **108,** 117003 (2012).
28. Camjayi, A., Haule, K., Dobrosavljević, V. & Kotliar, G. Coulomb correlations and the Wigner-Mott transition. *Nature Phys.* **4,** 932–935 (2008).
29. Nanda, B. R. K. & Satpathy, S. Electronic phases and phase separation in the Hubbard-Holstein model of a polar interface. *Phys. Rev. B* **83,** 195114 (2011).
30. Khalsa, G., Lee, B. & MacDonald, A. H. Theory of t_{2g} electron-gas Rashba interactions. Preprint at http://arxiv.org/abs/1301.2784 (2013).

Acknowledgements

We acknowledge stimulating conversations with L. Li, L. Balents, W. Cole, J. Mannhart, K. Moler, W. Pickett, S. Satpathy and N. Trivedi, and the support of DOE-BES DE-SC0005035 (S.B.), NSF-DMR-1006532 (O.E.) and NSF MRSEC DMR-0820414 (M.R.).

Author contributions

S.B., O.E. and M.R. contributed to the theoretical research described in the paper and the writing of the manuscript.

Additional information

Supplementary information is available in the online version of the paper. Reprints and permissions information is available online at www.nature.com/reprints. Correspondence and requests for materials should be addressed to M.R.

Competing financial interests

The authors declare no competing financial interests.